



MyD88 knockdown by RNAi prevents bacterial stimulation of tubeworm metamorphosis

Emily Darin^{a,1}, Morgan V. Farrell^{a,1}, Tatyana N. Ali^a, Josefa Rivera Alfaro^a, Kyle E. Malter^a, and Nicholas J. Shikuma^{a,2} 

Affiliations are included on p. 9.

Edited by Joan Strassmann, Washington University in St. Louis, St. Louis, MO; received March 13, 2025; accepted April 25, 2025

Diverse animals across the tree of life undergo the life-history transition of metamorphosis in response to bacteria. Although immunity has been implicated in this metamorphosis in response to bacteria, no functional connection has yet been demonstrated between immunity and metamorphosis. We investigated a host–microbe interaction involving a marine tubeworm, *Hydroides elegans*, that undergoes metamorphosis in response to *Pseudoalteromonas luteoviolacea*, a metamorphosis-inducing marine bacterium. By creating a marine bacteria–mediated RNA interference approach, we show that myeloid differentiation factor 88 (MyD88), a critical immune adaptor for Toll-like receptor and interleukin pathways, is necessary for the stimulation of metamorphosis in response to bacteria. In addition to a developmental role, we show that MyD88 is necessary for survival during exposure to the bacterial pathogen *Pseudomonas aeruginosa*, showing that *Hydroides* utilizes MyD88 during both development and an immune response. These results provide a functional characterization of the innate immune system involved in an animal's metamorphosis.

MyD88 | metamorphosis | immunity | bacteria | development

Life-history transitions in animals are significant developmental or behavioral shifts that occur throughout an organism's life. Prominent examples include the emergence of an individual from an egg, the transition of a tadpole undergoing metamorphosis into a frog, or sexual maturation such as puberty in humans (1–3). Although microbes have been linked to cellular and tissue development of many animals, including humans (4–6), examples of how microbes play critical roles in major life-history transitions remain scarce.

In the 1930s, Zobel and Allen first described a phenomenon whereby marine animals undergo the life-history transition of metamorphosis in response to bacteria (7). During this host–microbe interaction, swimming animal larvae identify a suitable location on the seafloor for settlement and metamorphosis by sensing and responding to surface-bound bacteria, transitioning from a planktonic to benthic lifestyle. Animals as diverse as sponges, corals, tubeworms, urchins, and ascidians have been shown to undergo metamorphosis in response to bacteria (8–10), suggesting that the linkage between metamorphic development and bacterial sensing is ancient and conserved. While the upregulation of genes implicated in immune activation has been observed during metamorphosis across diverse phyla (11–16), the necessity of the immune system for mediating animal metamorphosis in response to bacteria has not been demonstrated for any animal.

Toll-like receptors (TLRs) and myeloid differentiation factor 88 (MyD88) play important roles during the development and/or immune response of many animals. For example, nine different TLRs are utilized for either embryonic development, dorsal ventral symmetry, heart and muscle formation, or bacterial defense in *Drosophila melanogaster* (17). The TLR/MyD88 signaling pathway is required for pathogen defense and bacterial colonization in Hydra and *Drosophila* (18, 19). The model annelid tubeworm, *Hydroides elegans*, undergoes metamorphosis in response to specific bacteria (e.g. *Pseudoalteromonas luteoviolacea*) and is ideally suited to investigate whether innate immunity is critical for metamorphosis in response to bacteria (20–22).

Results

Bacterial Feeding and RNA Interference (RNAi) for Gene Knockdown in *Hydroides*.

Bacteria expressing double-stranded RNA (dsRNA) have been shown to be an effective delivery strategy for employing RNAi in model invertebrates such as bacterivorous nematodes and freshwater planarians (23–25). Similarly, *Hydroides* larvae and adults filter food from the water column and their growth has been shown to be supported by feeding on bacteria (26). We therefore sought to develop a strategy for performing RNAi with *Hydroides* by feeding them environmental bacteria producing dsRNA (Fig. 1A). By

Significance

Metamorphosis is a critical life-history transition in many animals, yet its underlying molecular mechanisms, particularly in response to environmental bacteria, remain poorly understood. This study provides a functional link between the innate immune system and metamorphosis, demonstrating that the immune adaptor protein MyD88 (myeloid differentiation factor 88) is required for bacterial-induced metamorphosis in the marine tubeworm *Hydroides elegans*. Using a newly developed bacterial-mediated RNA interference approach, we show that MyD88 is not only essential for metamorphosis in response to stimulatory bacteria but also for survival against a bacterial pathogen. These findings suggest that immune signaling pathways may regulate both development and host–microbe interactions across diverse animal species, expanding our understanding of how immunity contributes to fundamental biological transitions.

Competing interest statement: E.D., M.V.F. and N.J.S. are co-inventors on provisional US patent application serial number 63/687,110, entitled “Genetically Engineered Marine Bacteria for Biomaterial Production, Probiotic Use in Aquaculture and Marine Environmental Restoration” and assigned to San Diego State University Research Foundation.

This article is a PNAS Direct Submission.

Copyright © 2025 the Author(s). Published by PNAS. This open access article is distributed under [Creative Commons Attribution-NonCommercial-NoDerivatives License 4.0 \(CC BY-NC-ND\)](https://creativecommons.org/licenses/by-nc-nd/4.0/).

¹E.D. and M.V.F. contributed equally to this work.

²To whom correspondence may be addressed. Email: nshikuma@sdsu.edu.

This article contains supporting information online at <https://www.pnas.org/lookup/suppl/doi:10.1073/pnas.2505805122/-/DCSupplemental>.

Published June 2, 2025.

searching the genome and transcriptome (14), we determined that *Hydroïdes* possesses and expresses the molecular machinery critical for RNAi (*SI Appendix, Table S1*) (23).

To identify a strain of bacteria that serves as a food source without stimulating metamorphosis, we exposed *Hydroïdes* larvae to a series of five strains of marine bacteria. Of those bacteria tested, *P. mandapamensis* 4.11, *P. mandapamensis* 4.16, and *V. harveyi* did not induce metamorphosis (27) (Fig. 1*B*). When tested for their ability to sustain the growth of *Hydroïdes* from zygote to mature (competent) larva, *P. mandapamensis* 4.11 supported larval growth to competency at a level comparable to the traditional algal food *Isochrysis galbana* (21, 28) (*SI Appendix, Fig. S1A*). *Hydroïdes* did not grow or survive when exposed to *Escherichia coli* HT115, the strain used for RNAi through feeding in *Caenorhabditis elegans* nematodes (29). We found that *P. mandapamensis* 4.11 was amenable to genetic engineering, and the growth of *P. mandapamensis* 4.11 containing a broad-host-range plasmid (pDS-gfp) used for genetic manipulation was similar to the growth of *P. mandapamensis* 4.11 wild type (*SI Appendix, Fig. S1B*). When fluorescently tagged with an mRuby protein, *P. mandapamensis* 4.11 could be visualized within the *Hydroïdes* larval gut (Fig. 1*C*).

To determine whether *Hydroïdes* is amenable to RNAi gene knockdown via bacterial feeding, we transformed *P. mandapamensis* 4.11 with a plasmid (30–32) containing a 180 bp fragment of the *Hydroïdes atubulin* gene (TCONS_00033662, *SI Appendix, Table S2*) flanked by two constitutive CP25 promoters (pDS- α tubulin). Upon feeding *Hydroïdes* with *P. mandapamensis* pDS- α tubulin, we observed a loss of the swimming ciliary band while *Hydroïdes* larvae fed *P. mandapamensis* expressing dsRNA targeting a 200 bp fragment of *gfp* (pDS-gfp), a gene that does not occur in the *Hydroïdes* genome, showed no loss of the ciliary band (Fig. 2*A* and *B*). Visualization and quantification of *atubulin* expression using hybridization chain reaction (HCR) and qPCR confirmed the knockdown of *atubulin* along

the *Hydroïdes* ciliary band (prototroch) (Fig. 2*D, E*, and *G*). To test the specificity of RNAi knockdown, we fed *Hydroïdes* larvae *P. mandapamensis* with an RNAi plasmid targeting a second gene, a 270 bp fragment of the *Hydroïdes* carbonic anhydrase 1 (*CA1*) gene (TCONS_00094394, pDS-CA1, *SI Appendix, Table S2*), which is involved in tube building and expressed in a distinct anatomical location within the larval collar tissue, below the ciliary band (33). HCR and qPCR confirmed the knockdown of *CA1* in larvae fed pDS-CA1 while the expression in larvae fed pDS- α tubulin or pDS-gfp was unaffected (Fig. 2*C, F*, and *H*). Corresponding α tubulin immunostaining was reduced in larvae fed *P. mandapamensis* pDS- α tubulin compared to larvae fed *P. mandapamensis* pDS-gfp or pDS-CA1 (Fig. 2*I* and *SI Appendix, Fig. S1 C–E*). These results indicate that *Hydroïdes* is amenable to gene-specific RNA interference via feeding of *P. mandapamensis* expressing dsRNA.

***Hydroïdes* Requires MyD88 to Undergo Metamorphosis in Response to Bacteria.** We next analyzed the genome and transcriptome of *Hydroïdes* (14) and identified a set of genes implicated in the MyD88/TLR and nuclear factor kappa B (NF- κ B) pathways (*SI Appendix, Table S2*). We found significant similarities among invertebrate and human genes, including a single myeloid differentiation primary response 88 (*MyD88*) gene, two TNF receptor-associated factor 3 (*TRAF3*) genes, five I κ B (NF- κ B inhibitor, *I κ B*) genes, one I κ B kinase (*IKK*) gene, two REL genes, and one NF- κ B gene (*SI Appendix, Fig. S2*). All identified genes were found to be expressed in competent larval animals (*SI Appendix, Table S2*), suggesting that *Hydroïdes* possesses a functional MyD88/TLR pathway.

Because of its role in both development and immunity in other organisms, we focused on the key adaptor protein MyD88. To test whether *Hydroïdes* requires *MyD88* to undergo metamorphosis in response to bacteria, we created pDS-MyD88 containing a 200 bp

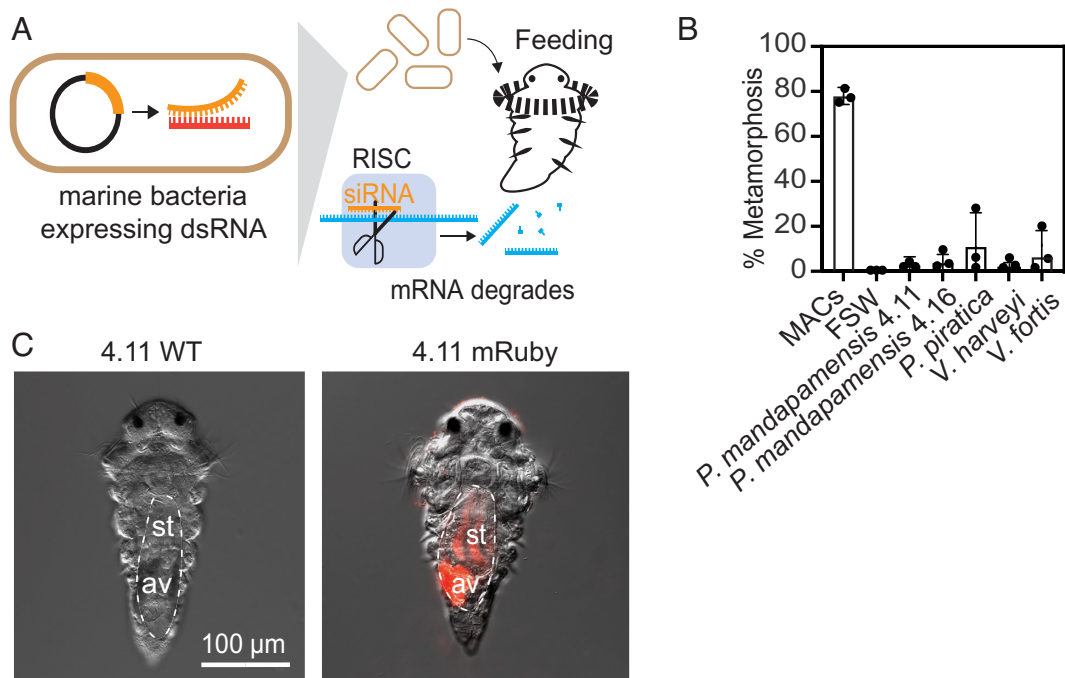


Fig. 1. *Hydroïdes* larvae feed on genetically modified marine bacteria. (A) Model of double-stranded RNA (dsRNA) delivery via bacterial feeding to *Hydroïdes* larvae. The RNA interference (RNAi) plasmid is carried by a feeder bacterium that serves as a food source but does not stimulate metamorphosis. The tubeworm’s RNA-Induced Silencing Complex (RISC) cleaves the dsRNA into small RNA fragments (siRNA), leading to targeted mRNA degradation. (B) Graph of *Hydroïdes* metamorphosis after 24 h bacterial exposure to MACs (Metamorphosis-Associated Contractile structures), artificial seawater (ASW), *Photobacterium mandapamensis* strains 4.11 and 4.16, *Pseudoalteromonas piratica*, *Vibrio harveyi*, and *Vibrio fortis*. Data are generated from three independent experiments ($n = 3$). Error bars represent SD. (C) Micrograph of *Hydroïdes* larvae fed *P. mandapamensis* 4.11 wild-type or *P. mandapamensis* 4.11 mRuby-tagged bacteria. Dashed line outlines stomach (st) and anal vesicle (av) in *Hydroïdes* larvae.

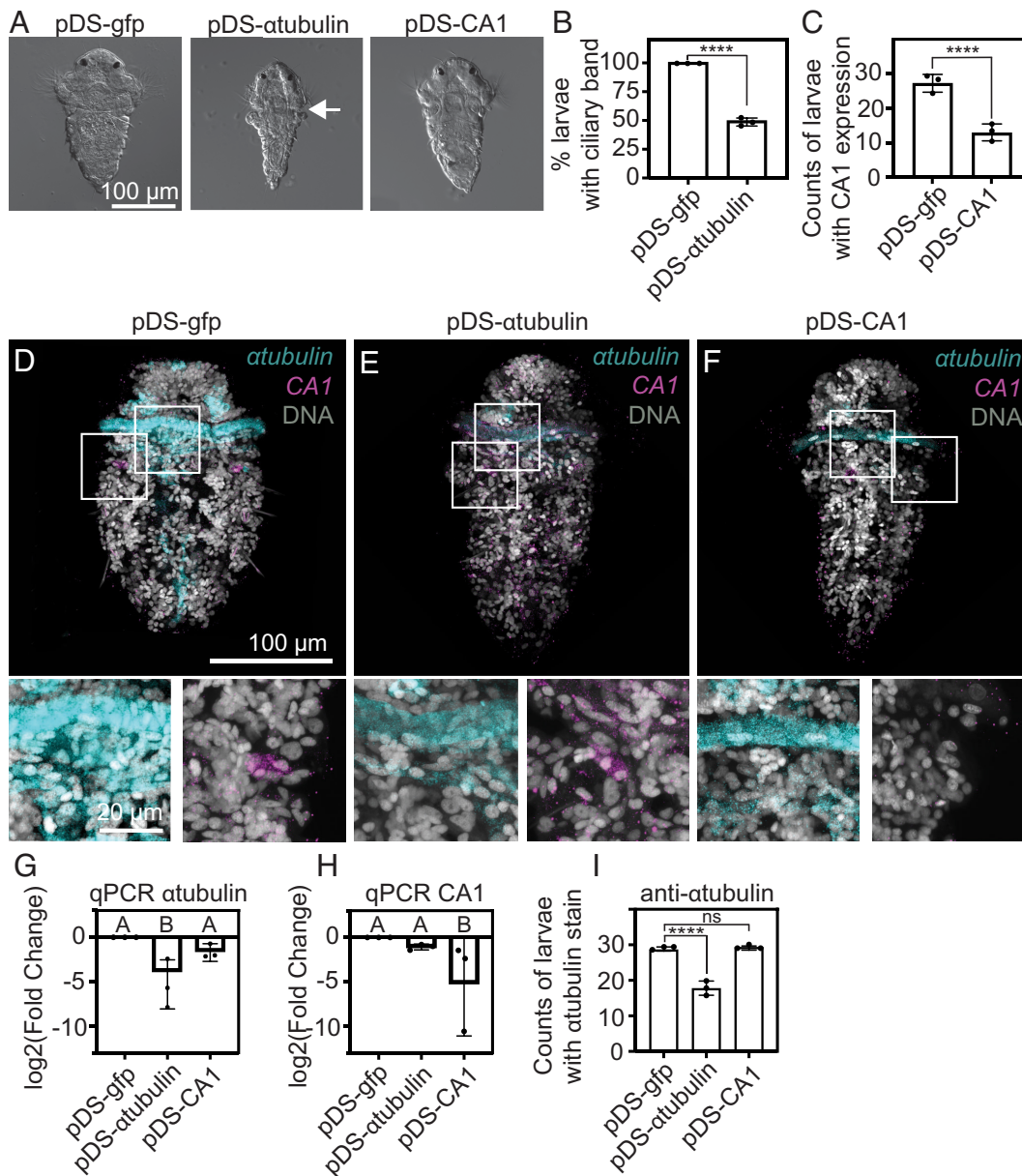


Fig. 2. Gene-specific knockdown in *Hydroides* via bacteria feeding and RNA interference. (A) DIC micrographs of *Hydroides* larvae after 24-h feeding *P. mandapamensis* 4.11 with pDS-gfp, pDS- α tubulin, or pDS-CA1. The white arrow indicates the location of ciliary band loss. (B) Percent larvae fed *P. mandapamensis* pDS-gfp or pDS- α tubulin with ciliary band after 24 h. Data are generated from three independent experiments ($n = 3$) with an average of 300 larvae scored for each treatment (**** $P < 0.0001$, calculated using a chi-square test with Yates' correction). Error bars represent SD. (C) Counts of larvae with CA1 HCR expression 24 h after feeding *P. mandapamensis* pDS-gfp or pDS-CA1. Data are generated from an average of 30 larvae scored for each of three independent experiments ($n = 3$) (**** $P < 0.0001$, calculated using a chi-square test with Yates' correction). Error bars represent SD. (D) HCR of *atubulin* (turquoise), CA1 (magenta), and DNA (DAPI, gray) in larvae fed *P. mandapamensis* pDS-gfp after 24 h. Lower Left 3.4 \times zoomed in panel of ciliary band and Lower Right 3.4 \times zoomed in panel of CA1 gland for pDS-gfp exposed larvae. (E) HCR of *atubulin* (turquoise), CA1 (magenta), and DNA (DAPI, gray) in larvae fed *P. mandapamensis* pDS- α tubulin after 24 h. Lower Left 3.4 \times zoomed in panel of ciliary band and Lower Right 3.4 \times zoomed in panel of CA1 gland for pDS- α tubulin exposed larvae. (F) HCR of *atubulin* (turquoise), CA1 (magenta), and DNA (DAPI, gray) in larvae fed *P. mandapamensis* pDS-CA1 after 24 h. Lower Left 3.4 \times zoomed in panel of ciliary band and Lower Right 3.4 \times zoomed in panel of CA1 gland for pDS-CA1 exposed larvae. (G) qPCR of the *Hydroides atubulin* gene in larvae fed *P. mandapamensis* pDS-gfp, pDS- α tubulin, or pDS-CA1 after 24 h. Data are generated from ~500 larvae in each of three technical replicates for each of three independent experiments ($n = 3$). Fold change values calculated using the DDCT method (Letters represent one-way ANOVA and Tukey post hoc test results, $P < 0.001$). Error bars represent SD. (H) qPCR of the *Hydroides CA1* gene in larvae fed *P. mandapamensis* pDS-gfp, pDS- α tubulin, or pDS-CA1 after 24 h. Data are generated from ~500 larvae in each of three technical replicates for each of three independent experiments ($n = 3$). Log2 fold change values calculated using the DDCT method (Letters represent one-way ANOVA and Tukey post hoc test results, $P < 0.001$). Error bars represent SD. (I) Counts of larvae with anti- α tubulin staining after feeding *P. mandapamensis* pDS-gfp, pDS- α tubulin, or pDS-CA1 for 24 h. The graph is an average of three biological replicates ($n = 3$) with 30 larvae per replicate per treatment (chi-square test with Yates' correction, **** $P < 0.0001$ comparing pDS-gfp to pDS- α tubulin, n.s. comparing pDS-gfp to pDS-CA1). Error bars represent SD.

fragment of the *Hydroides MyD88* gene (TCONS_00085995, SI Appendix, Fig. S3). We then fed *Hydroides* larvae with *P. mandapamensis* pDS-MyD88 for 24 h followed by stimulating the larvae to undergo metamorphosis with a known bacterial stimulant MACs (metamorphosis associated contractile structures) from *P. luteoviolacea* (14, 20, 22). Upon stimulation by MACs, *MyD88* knockdown

animals were unable to undergo metamorphosis in response to MACs in comparison to larvae fed *P. mandapamensis* pDS-gfp (Fig. 3 A, B, and D). Larvae exposed to a MyD88 inhibitor (TJ-M2010-5) (34) were similarly unable to undergo metamorphosis (Fig. 3 C and D). *MyD88* expression quantified using HCR counts and qPCR decreased in larvae fed *P. mandapamensis* pDS-MyD88 for 24 h and

subsequently exposed to MACs (Fig. 3 E, F, and H), while animals fed *P. mandapamensis* pDS-gfp showed expression of *MyD88* beneath the swimming ciliated band, ventral nerve cord, and cerebral ganglia of the nervous system (Fig. 3G). These results demonstrate that *MyD88* is critical for *Hydroides* to undergo metamorphosis in response to bacteria.

MyD88 Regulates Genes Implicated in Immunity and Development.

To determine the effect of *MyD88* knockdown on gene network regulation, we identified a set of four genes implicated in immunity and development, including interleukin 17 (IL17), Runt-related

transcription factor (RUNX), Fos, and Nuclear Hormone Receptor 2 (NHR2) (SI Appendix, Table S2). We focused on these genes because all four are expressed in *Hydroides* larvae undergoing metamorphosis (14). Moreover, the promoters of *IL17*, *Fos*, and *RUNX* contain predicted NF- κ B binding sites and *RUNX* contains an AP-1 binding site (SI Appendix, Table S3). When qPCR and HCR were performed on larvae fed *P. mandapamensis* pDS-gfp or pDS-MyD88 for 24 h and subsequently exposed to MACs for 30 min, we found that the expression of *IL17*, *RUNX*, *Fos*, and *NHR2* was significantly downregulated in *MyD88* knockdown larvae when compared to *gfp* knockdown larvae (Fig. 4A), and counts of larvae with HCR

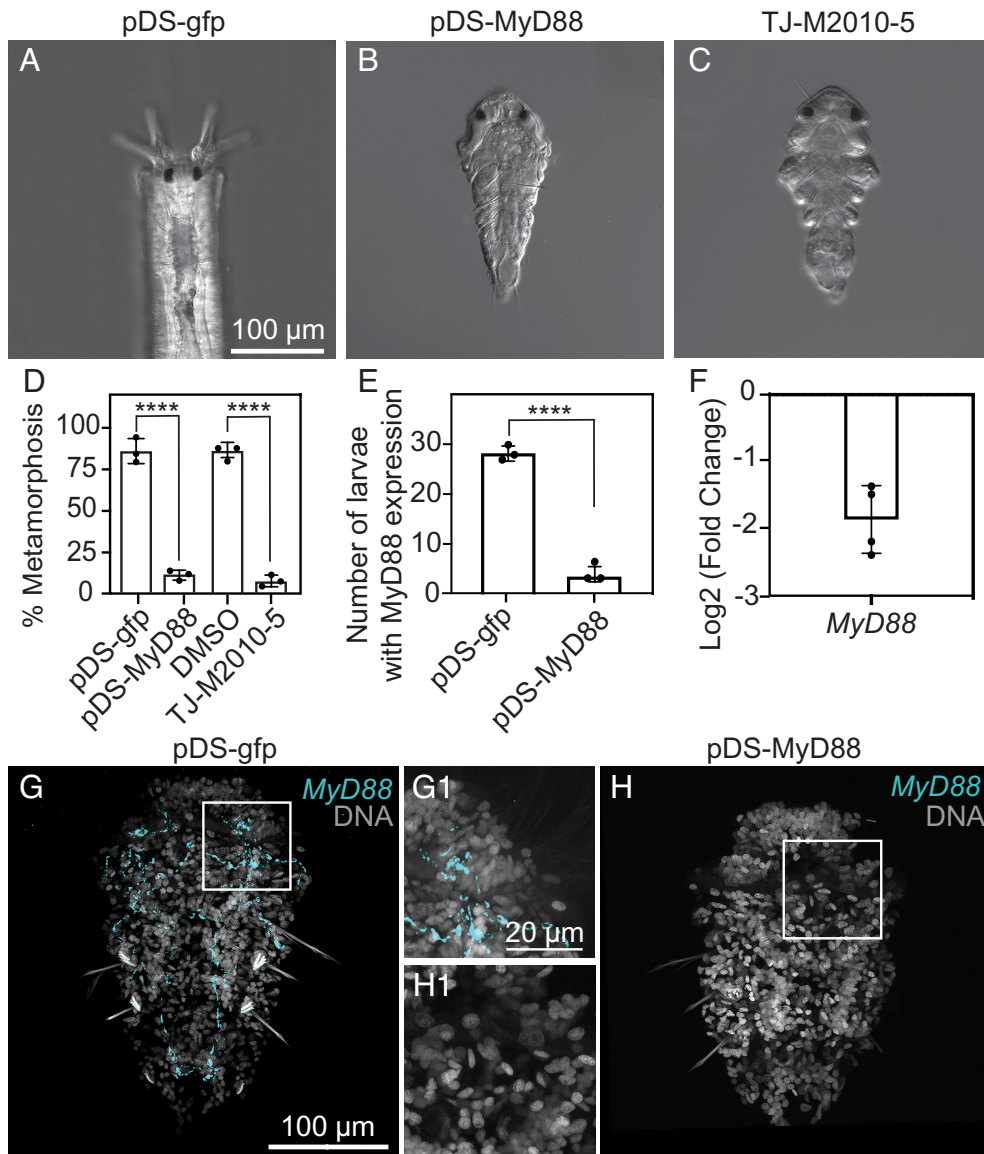


Fig. 3. MyD88 knockdown inhibits metamorphosis. (A–C) DIC micrographs of *Hydroides* larvae after 24-h feeding on *P. mandapamensis* (A) pDS-gfp or (B) pDS-MyD88 or (C) exposure to a MyD88 inhibitor (TJ-M2010-5) and subsequent 24 h exposure to MACs. (D) Percent metamorphosis after 24-h feeding *P. mandapamensis* pDS-gfp, *P. mandapamensis* pDS-MyD88, DMSO solvent (0.05%) or exposure to a MyD88 inhibitor (TJ-M2010-5) and subsequent 24 h exposure to MACs. Data are generated from three independent experiments (n = 3) with an average of 300 larvae scored for each treatment. Data are analyzed using a chi-square test with Yates' correction (****P < 0.0001). Error bars represent SD. (E) Counts of larvae showing *MyD88* HCR expression after 24-h feeding *P. mandapamensis* pDS-gfp or *P. mandapamensis* pDS-MyD88 and subsequent 5 min exposure to MACs. The graph is an average of three biological replicates (n = 3) with 30 larvae per replicate per treatment. Data are analyzed using a chi-square test with Yates' correction (***P < 0.001). Error bars represent SD. (F) qPCR log2 fold change values of *MyD88* after 24-h feeding *P. mandapamensis* pDS-gfp or *P. mandapamensis* pDS-MyD88 and subsequent 30 min exposure to MACs. Results were calculated using the DDCT method across four biological replicates (n = 4) with ~500 larvae per replicate per treatment. Error bars represent SD. (G) HCR of *MyD88* (turquoise) and DNA (DAPI, gray) in larvae after 24-h feeding *P. mandapamensis* pDS-gfp and subsequent exposure to MACs for 5 min. Images were taken with an oil objective at 63x. (G1) 2.85x zoom. (H) HCR of *MyD88* (turquoise) and DNA (DAPI, gray) in larvae after 24-h feeding *P. mandapamensis* pDS-MyD88 and subsequent exposure to MACs for 5 min. Images were taken with an oil objective at 63x. (H1) 2.85x zoom.

expression corroborated these observations (Fig. 4B). When HCR expression was observed with fluorescence microscopy, the anatomical location of expression was different for each gene and less expression was observed in the *MyD88* knockdown animals. *IL17* expression localized to the swimming cilia of the prototroch (Fig. 4C and D). *RUNX* expression was present in the gut, beneath the ciliary band and cerebral ganglia (Fig. 4E and F). *Fos* expression was observed throughout the larval body and was concentrated near the anterior region of the head (Fig. 4G and H). *NHR2* expression localized to the larval head and beneath the ciliary band (Fig. 4I and J).

These results indicate that MyD88 plays a role in regulating genes implicated in development and immunity during the stimulation of metamorphosis.

MyD88 Plays Dual Roles in Pathogen Response and Metamorphosis. To determine whether MyD88 plays a canonical role in immune pathway activation, we exposed larvae fed *P. mandapamensis* with pDS-gfp or pDS-MyD88 to the bacterial pathogen, *Pseudomonas aeruginosa* PA14, which has been reported to cause disease in plants, nematodes, insects, mice, and

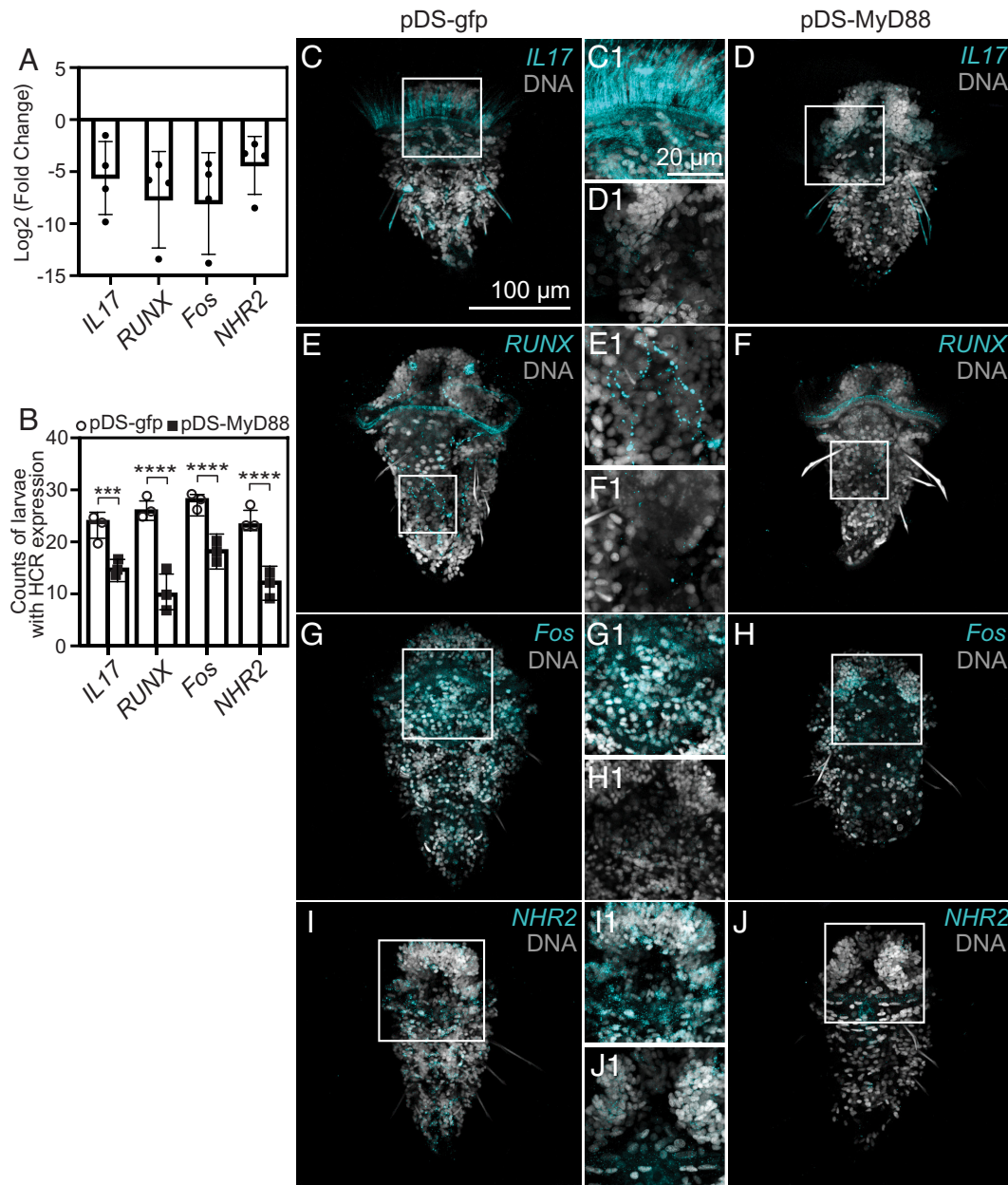


Fig. 4. MyD88 activates immune and developmental genes upon the stimulation of metamorphosis by bacteria. (A) Graph of qPCR log₂ fold change values of *IL17*, *RUNX*, *Fos*, and *NHR2* in larvae fed *P. mandapamensis* pDS-gfp or pDS-MyD88 for 24 h and then exposed to MACs for 30 min. Results were calculated using the DDCT method across four biological replicates (n = 4) with ~500 larvae per replicate per treatment. Error bars represent SD. (B) Graph of expression counts of *NHR2*, *IL17*, *RUNX*, and *Fos* using HCR in larvae fed *P. mandapamensis* pDS-gfp or pDS-MyD88 for 24 h and then exposed to MACs for 30 min. The graph is an average of three biological replicates (n = 3) with 30 larvae per replicate per treatment, data analyzed using the chi-square test with Yates' correction (****P < 0.0001, ***P < 0.001). Error bars represent SD. (C and D) HCR of *IL17* (turquoise) and DNA (DAPI, gray) in larvae after 24-h feeding *P. mandapamensis* (C) pDS-gfp or (D) pDS-MyD88 and subsequent exposure to MACs for 30 min. Images were taken with an oil objective at 63x. (C1 and D1) 2.85x zoom. (E and F) HCR of *RUNX* (turquoise) and DNA (DAPI, gray) in larvae after 24-h feeding *P. mandapamensis* (E) pDS-gfp or (F) pDS-MyD88 and subsequent exposure to MACs for 30 min. Images were taken with an oil objective at 63x. (E1 and F1) 2.85x zoom. (G and H) HCR of *Fos* (turquoise) and DNA (DAPI, gray) in larvae after 24-h feeding *P. mandapamensis* (G) pDS-gfp or (H) pDS-MyD88 and subsequent exposure to MACs for 30 min. Images were taken with an oil objective at 63x. (G1 and H1) 2.85x zoom. (I and J) HCR of *NHR2* (turquoise) and DNA (DAPI, gray) in larvae after 24-h feeding *P. mandapamensis* (I) pDS-gfp or (J) pDS-MyD88 and subsequent exposure to MACs for 30 min. Images were taken with an oil objective at 63x. (I1 and J1) 2.85x zoom.

humans (35–37). When exposed to four of six densities (OD600 of 0.19, 0.38, 0.75, 1.5) of *P. aeruginosa* PA14, the survival of *Hydroïdes* fed *P. mandapamensis* pDS-MyD88 was significantly reduced (Fig. 5). In contrast, the survival of *Hydroïdes* fed *P. mandapamensis* pDS-gfp showed no difference with larvae exposed to artificial seawater alone. These results demonstrate that MyD88 is critical for survival of *Hydroïdes* in response to a bacterial pathogen.

Discussion

Connecting MyD88 with Animal Metamorphosis. Invertebrates from across the animal tree of life undergo metamorphosis in response to bacteria (e.g., sponges, corals, tubeworms, urchins, tunicates), suggesting that metamorphosis in response to bacteria sensing is an ancient and conserved process (8, 14, 38). In mussels, ascidians, and frogs, genes often associated with immunity are modulated during metamorphosis and the immune system has been hypothesized previously to be critical for metamorphosis (11, 12, 39–41). The conservation of metamorphosis in response to bacteria sensing in diverse animals prompted us to search for a connection between immunity and metamorphosis.

Immunity has historically been studied in the context of eliminating pathogens and controlling commensal colonization. However, MyD88 is a critical adaptor protein for multiple immune pathways and has also been shown to mediate animal development. In *D. melanogaster*, MyD88 drives dorsoventral patterning during embryogenesis (42), in addition to its role in fighting fungal and bacterial infections (19). In mice, MyD88 deficiency causes abnormal brain development, including altered neuronal branching, and behavior changes (43).

Hydroïdes possesses an intact innate immune system (Fig. 6 and *SI Appendix, Table S2*) and we show via RNAi knockdown that the MyD88 adaptor protein is required for metamorphosis in response to bacteria. Furthermore, MyD88 regulates genes implicated in both immunity and development during metamorphosis in response to bacteria (Fig. 4). Specifically, MyD88 regulates a *Hydroïdes* *IL17* homolog, which has been shown to play central roles in immune inflammation in response to pathogens by regulating inflammation in invertebrates as well as specific immune cell type responses in vertebrates (44–47). MyD88 regulates *Fos*, which forms a portion of the AP-1 complex and is activated by MAPK in the MyD88-dependent signaling pathway (48). During development and immune response, *Fos* is utilized to regulate differentiation, proliferation, and apoptosis (49, 50). In *Hydroïdes*, *Fos* is activated during *Hydroïdes* metamorphosis in response to MACs (14), and our results here demonstrate the regulation of *Fos* by MyD88. MyD88 also regulates two developmental genes *RUNX* and *NHR2* (Fig. 4). In *Drosophila*, Runt functions as a pair rule transcription factor for both embryonic pattern formation development and neuronal development (51), and in mammals, the mammalian RUNX domain plays a central role in development of blood and bone (52). Here, we found that *Hydroïdes* *RUNX* may be expressed in the nervous system. *NHR2* is a nuclear hormone receptor gene previously described to be activated during *Hydroïdes* metamorphosis (53), which fits with the canonical role of nuclear hormone receptors in growth, differentiation, reproduction, and morphogenesis of vertebrates (54). Overall, our results demonstrate that genes implicated in both immunity and development play a central role in *Hydroïdes* metamorphosis.

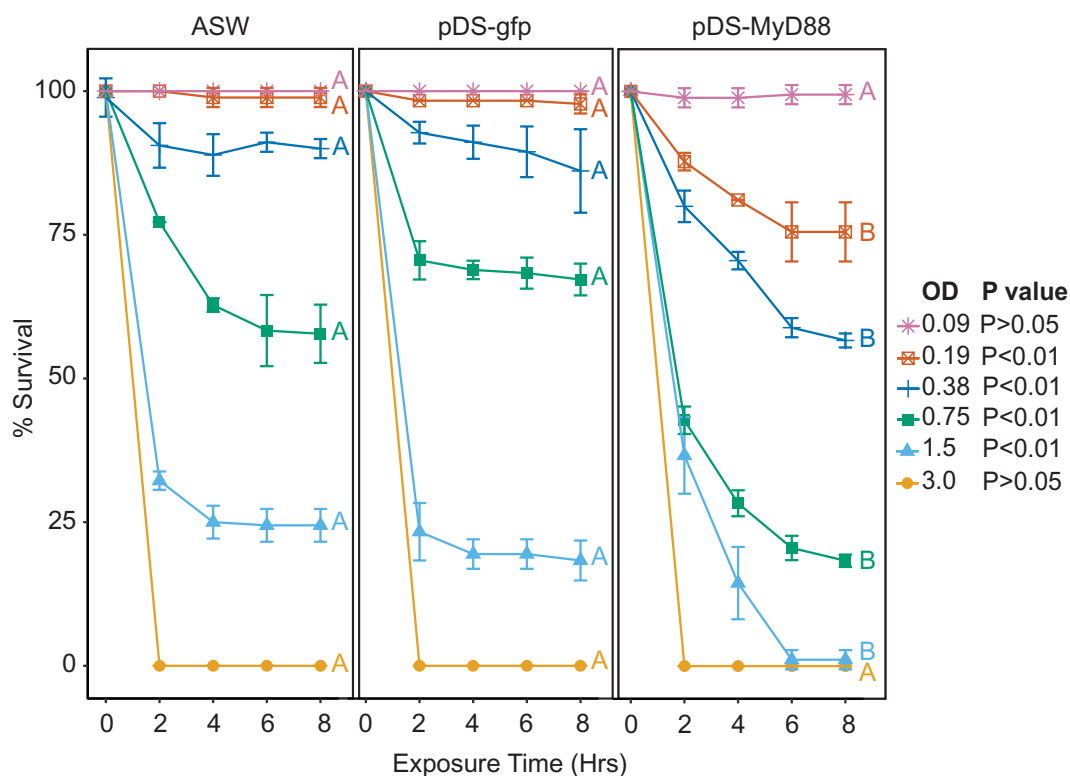


Fig. 5. *Hydroïdes* require MyD88 for bacterial pathogen defense. *Hydroïdes* larvae were exposed to ASW, *P. mandapamensis* pDS-gfp, or *P. mandapamensis* pDS-MyD88 for 24 h. Subsequently, larvae were exposed to *P. aeruginosa* PA14 and scored for survival over 8 h. The Y-axis represents % survival at each timepoint on the x-axis (0, 2, 4, 6, and 8 h). The graph is an average of three biological replicates ($n = 3$) with 30 larvae per replicate per treatment. One-way ANOVA was performed against all six treatments at each individual optical density averaged across the 8 h. A Tukey post hoc test was performed to test for differences between each treatment. Letters denote statistically different treatments. Error bars represent SD.

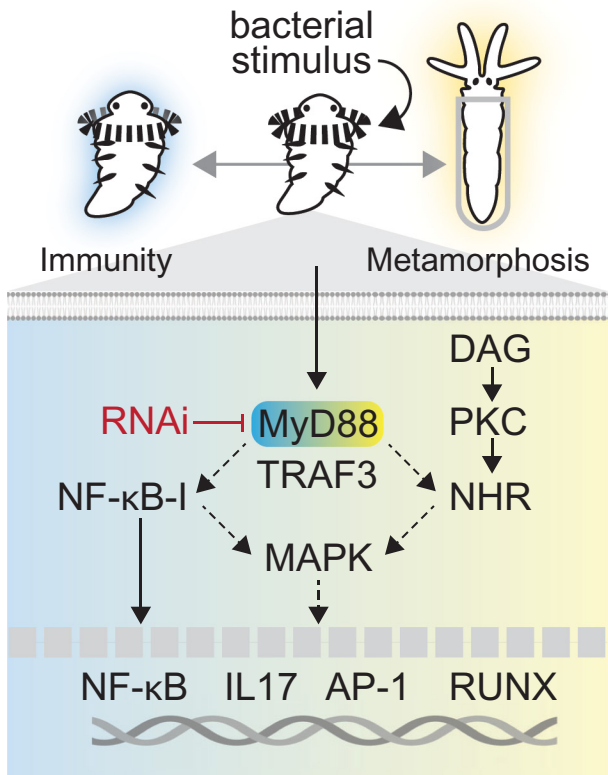


Fig. 6. Model of *Hydroides* immune and developmental regulation during metamorphosis. Our findings support the following model whereby the MyD88 pathway mediates the sensing of a bacterial stimulus in *Hydroides* larvae and operates at the interface of both the pathogen and metamorphosis response. Upon stimulation by *P. luteoviolacea* MACs, *IL17*, *RUNX*, and *NHR2* are positively regulated by MyD88 and their expression localizes to the cilia, nervous system, and/or cerebral ganglia of *Hydroides* larvae. In a parallel pathway, diacylglycerol (DAG) and Protein Kinase C (PKC) activate NHR1 and NHR2 (53). MyD88 also activates p38 and JNK MAPK signaling (14, 53, 55). When challenged with *P. aeruginosa*, MyD88 mediates a bacterial pathogen response through a yet unknown pathway.

Bacteria Sensing and Metamorphosis Response. For all animals, the sensing of bacteria is critical for mounting an appropriate response. For *Hydroides* larvae, environmental bacteria are hypothesized to serve as environmental indicators of a preferable habitat (38). We observed that MyD88 is expressed in the ciliated band and cerebral ganglia of *Hydroides* larvae (Fig. 3G) and MyD88 regulates the expression of *IL17*, *RUNX*, *Fos*, and *NHR2*, which localize to the cilia, cerebral ganglia, and nervous system of the larval animal (Fig. 4). Using HCR, we detected *IL17* mRNA signal in the swimming cilia of the prototroch—an unexpected localization given that cilia are not typically considered sites of mRNA accumulation. Although this pattern could result from technical artifacts—such as nonspecific probe binding, accumulation of amplification products within the glycocalyx, or mRNA leakage from compromised cells—the absence of signal in negative controls, along with the distinct staining profiles of other HCR probes, suggests that the observed localization may warrant further investigation. Interestingly, mRNA localization to cilia has been documented in other systems, where it may facilitate localized translation or signaling (56). We observed that the primary anatomical location of interaction between larvae and the bacterial stimulant MACs is at the larval ciliated band (prototroch and metatroch) (55), implicating larval swimming cilia as a hub for the stimulation of *Hydroides* metamorphosis by bacteria.

Our results are congruent with findings of TLRs regulating neurogenesis in nematodes (57, 58) and mammals (59) and parallel other host–microbe systems where the spatial localization of

TLR and MyD88 components plays critical roles in mounting an appropriate response. For example, in human intestinal epithelial cells, inflammatory signaling occurs from basolaterally expressed TLR9, allowing the epithelium to identify bacteria that have penetrated the host epithelial barrier (60). In zebrafish, TLR4 and MyD88 modulate the expression and activity of intestinal alkaline phosphatase, which aids in detoxification of lipopolysaccharide and prevents over inflammation in response to commensal microbes (61). The spatial localization of MyD88, immune, and developmental genes in *Hydroides* suggests that environmental sensing in larvae occurs at the ciliary interface and signaling involves the larval nervous system.

In *Hydroides* and many other marine animals, metamorphosis is linked with stimulation by bacteria (8, 14). And in the present work, we provide evidence functionally connecting MyD88 with metamorphosis. Currently, we do not yet know whether or how the MyD88 pathway is interconnected with the mechanisms of bacteria sensing leading to metamorphosis. However, our results contrast with metamorphosis in *Drosophila* where the generation of germ-free lines demonstrates that metamorphosis does not require bacteria (62, 63) and that *Drosophila* metamorphosis can occur in the absence of a functional *MyD88* gene (19). Determining whether and how *Hydroides* sensing of bacteria links with the MyD88 and developmental pathways will help to determine how developmental and immunity pathways connect during the sensing of bacteria and stimulation of metamorphosis. Such findings will also lead to a broader understanding of the mechanisms of metamorphosis in response to bacteria in other diverse animal phyla.

Engineered Bacteria for RNAi Delivery. The strategy of RNAi by bacterial feeding has been successfully applied in insects, planarians, and nematodes (24, 64, 65). However, instances of RNAi via feeding remain scarce in model marine invertebrates. Our results of RNAi via bacterial feeding in *Hydroides* allows for knockdown during specific stages of an animal's life history, opening up the possibility of investigating gene function beyond embryogenesis, such as during metamorphosis and other developmental transitions when direct genetic modification is not possible. Diverse marine proteobacteria have been modified to carry broad-host-range plasmids (30), and other bacterial species could therefore likely be employed for RNAi delivery as well. Moreover, our results provide a roadmap for applying RNAi via bacterial feeding in other aquatic invertebrates, many of which do not yet have developed functional genetic approaches. In addition to answering fundamental research questions, RNAi has been suggested as an effective strategy for insect pest control of crops, especially because it can serve as an alternative to broad-spectrum pesticides (66). Our results raise the possibility that RNAi delivery via environmental bacteria could be an effective strategy for aquatic applications such as biofouling management, aquaculture animal disease treatment or improving production or in the restoration of degraded environments such as coral reefs.

Conclusion

Based on our results, we propose that the MyD88 innate immune pathway is a critical feature of the life-history transition of metamorphosis in response to bacteria. The sensing of and response to stimulatory bacteria via the immune system is likely critical for the life history and ecology of animals from diverse phyla. The innate immune system, therefore, may play a greater role in both pathogen response and development throughout the animal kingdom than previously recognized.

Materials and Methods

Identification of Gene Homology. Gene homologs were identified in the *H. elegans* genome (14) by using translated nucleotide BLAST (tblastn) against Taxa-ID: 216498. Initial blast search was conducted with key conserved domains of human immune proteins using NCBI Conserved Protein Domain Family Database (<https://www.ncbi.nlm.nih.gov/Structure/cdd/cdd.shtml>). Hits from the initial BLAST search ($E < 10^{-6}$) were screened for duplications or fragments of genes by aligning the protein level sequences and consolidating hits that have over 95% similarity (67). Further screening was done to determine whether hits have all the necessary conserved protein domains using InterPro (<https://www.ebi.ac.uk/interpro/>). Proteins lacking key domains were eliminated as homologs. Only for the case of TRAF3 where many putative homologs were identified we used gene expression as elimination criteria. Expression was evaluated by transcriptome data of gene expression before exposure to MACs and 30-min after (14). Hits that did not have an increase in expression (FPKM) after exposure to MACs were eliminated as homologs. A phylogenetic analysis was performed to determine the relationship between *Hydroïdes* genes and genes from other representative animal taxa. Protein sequences of *Hydroïdes* homologs were aligned with *D. melanogaster*, *Homo sapiens*, *Strongylocentrotus purpuratus*, *Hydra vulgaris*, *Crassostrea virginica*, *Magallana gigas*, *C. elegans*, and/or *Mizuhopecten yessoensis* using Clustal Omega (ClustalO v1.2.3) alignment with mBed algorithm. Protein alignment was then used to create a Maximum Likelihood tree using IQ-Tree v1.6.12 finding the best fit model. Branch support was calculated with 1000 bootstrap replicates. Phylogenetic trees were visualized in FigTree v1.4.4.

Hydroïdes Collection and Maintenance. *H. elegans* animals were collected from the Quivera Basin, San Diego, CA, and kept as described previously (20, 28). Gametes were spawned from adult animals and fertilized in 1L beakers with 0.45 μ M filtered ASW. Larvae were reduced to 5 larvae per mL at 24 h post fertilization and fed *Isochrysis* algae at an average of 60,000 cells per mL. Water changes were performed daily. Larvae were considered competent between days 6 and 8 as described previously (28).

Metamorphosis Assays. Metamorphosis assays were performed as described previously (53). Briefly, assays were performed in a 96-well plate with competent larvae spawned from three different mate pairs, each mate pair was treated as a separate biological replicate. The MyD88 inhibitor used in this work is TJ-M2010-5 (Med Chem Express, HY-139397) at a concentration of 0.005 mM. DMSO solvent (0.05%) in ASW was used as a vehicle control. Treatments included a 1:100 dilution of MACs and ASW as a control. Each treatment included three technical replicates. Larvae were exposed for 24 h and juveniles in each treatment were counted and divided by the total number of larvae to calculate a percentage. An average of the three technical replicates in each treatment was taken and then averaged across the three biological replicates. Data were analyzed using a chi-square test with Yates' correction in PRISM v10.

RNAi Plasmid Construction and Cloning. Golden Gate Assembly was performed to create the RNAi plasmids (30–32, 68). The backbone consisted of a GFP dropout flanked by BsaI cut sites. The Type-2 part consisted of a forward CP25 constitutive promoter and a reverse rnpB-T1 terminator (32). The Type-4 part consisted of a reverse CP25 promoter and forward rpoC terminator. The coding sequences were created as gBlocks, with a 180 to 400 bp fragment of the targeted gene (Integrated DNA Technologies, Coralville, IA). Golden Gate Assembly was performed with NEBridge Golden Gate Assembly Kit for BsaI-HF v2 (New England Biolabs, Catalog # E1601S) with 50 fmol of each plasmid used in the reaction. Reaction was run with the following thermocycler program 37 °C for 1 min, 16 °C for 1 min, repeat cycles 1 to 2 30 \times , 60 °C for 5 min. The assemblies were electroporated into SM10 λ pir cells, confirmed by colony PCR (EconoTaq PLUS Green, LGC Biosearch) with internal primers (*SI Appendix, Table S6*) and then electroporated into MFD λ pir cells for conjugation.

Production of MACs Extracts. MACs purification was carried out as described previously (69). Briefly, *P. luteoviolacea* H11 was struck out to single colonies onto Sea Water Tryptone (SWT) media (35.9 g/L Instant Ocean, 2.5 g/L tryptone, 1.5 g/L yeast extract, 1.5 mL/L glycerol, and 15 g/L agar) and grown at 25 °C overnight. A single isolated colony was inoculated into a 5 mL SWT culture and grown shaking overnight at 200 rpm in 25 °C. The culture was then inoculated 1:100 into a 50

mL SWT culture shaking overnight at 200 rpm in 25 °C. The 50 mL culture was centrifuged at 4 °C for 20 min at an rpm of 4,800. The supernatant was then removed and the pellet was resuspended in 5 mL of extraction buffer (20 mM Tris Base, 1 M NaCl, pH 7.5) and then centrifuged again at 4 °C for 20 min at an rpm of 4,800. This was repeated once more for a total of three times. After the final centrifugation, 3 mL was removed from the top of the supernatant. The MACs extract was then tested on competent larvae at a dilution of 1:100 to determine MACs efficacy. MACs were used within 24 h of production.

Bacterial Biparental Mating. *E. coli* donor strains MFD λ pir containing RNAi replicative plasmids were grown under antibiotic selection in LB (Miller, BD Difco) with 20 μ g/mL of gentamicin and 0.3 mM of Diaminopimelic acid (DAP). A single colony of MFD λ pir containing RNAi plasmids was inoculated and grown overnight in liquid culture at 37 °C shaking at 200 rpm. Marine bacteria strain *P. mandapamensis* 4.11 was inoculated with three colonies in Marine Broth (MB) 2216 (BD Difco) and grown overnight in liquid culture at 25 °C shaking at 200 rpm. Cultures were spun down (4,000 \times g for 10 min). All supernatant was removed from each culture and the pellets were resuspended in 150 μ L of MB. Donor and recipient cultures were mixed (200 μ L total volume) and spotted in 50 μ L spots onto MB agar plates and incubated overnight at 25 °C. The next day, each individual spot was scraped up and resuspended in 250 μ L of MB media. To wash the spots this process was repeated with the final resuspension in 100 μ L. The full 100 μ L was then plated onto MB agar plates with 200 μ g/mL of gentamicin. Colonies were PCR screened for the plasmid using internal primers (*SI Appendix, Table S6*).

Growing Larvae to Competence on Bacteria. Bacterial feeding assays were performed with larvae that were spawned from three different mate pairs, each mate pair was treated as a separate biological replicate. Larvae were separated into six technical replicates in 6-well cell culture plates with ASW. Bacterial strains (*V. harveyi*, *P. mandapamensis* 4.11, *P. mandapamensis* 4.16, *E. coli* HT115) were fed daily at an OD (Optical Density 600 nm) of 0.1. Control larvae were fed *I. galbana* algae daily. Larvae were water changed daily using a 20 μ m mesh basket. At 3 and 7 d post fertilization, larvae were counted on a dissection scope and scored precompetent, competent, or dead. Data were graphed as averages of three biological replicates ($n = 3$) and the error bars represent SD.

Larval RNAi Exposures. *P. mandapamensis* 4.11 containing RNAi plasmids were struck out on a MB agar plate with 200 μ g/mL gentamicin and grown at 25 °C overnight. A single colony was then inoculated into 25 mL of MB media with gentamicin. After 16 h of growth, cultures were spun down into a pellet and washed three times with 5 mL of ASW, and the optical density was then quantified using a Nanodrop. Larvae were fed bacteria at an OD of 0.25 for 24 h in ASW. Larvae were checked for abnormalities and competency before metamorphosis induction. Larvae were starved 24 h prior to feeding to ensure adequate feeding on bacteria.

Larval RNA Extractions. Competent larvae were exposed to a 1:100 dilution of MACs or ASW. Roughly 500 larvae were collected at 30 min of exposure and preserved in RNA Later (0.5 M EDTA, 1 M Sodium Citrate) for RNA extraction. Samples were kept at -80 °C and then placed on ice for RNA extraction. RNA was extracted from larvae using the Macherey Nagel RNA extraction kit (Catalog # 740955.50). Samples were kept on ice and washed with 1 mL of RNase free PBS and spun down with a manual centrifuge at 100 rpm for 30 s. This was repeated twice before larvae were lysed with the RNA extraction lysis buffer. After lysis and desalting and DNase removal step was performed, RNA was then washed and eluted in 30 μ L RNase free water. RNA was quantified using a Nanodrop, quality RNA was used with 260/230 and 260/280 ratios greater than 1.8.

cDNA Synthesis and qPCR. cDNA synthesis was performed on RNA samples using NEB Biolabs Protoscript II First Strand cDNA Synthesis kit (Catalog # E6560S). Each cDNA reaction was standardized to synthesize 1 μ g of RNA. Reactions were carried out at 42 °C for 1 h followed by 5 min at 85 °C. cDNA was kept at -80 °C for 48 h. qPCR was performed with exon-exon primers designed in PRIMER 3 and JBrowse. Genes analyzed were *atubulin*, *CA1*, *MyD88*, *IL17*, *RUNX*, *Fos*, and *NHR2*. *18S* and *GAPDH* were chosen as housekeeping controls. Each 20 μ L qPCR was created using 10 μ L of PRIMA qMAX mix (Catalog # PR2120-H-S), 50 ng of cDNA and 3.5 μ L of forward and reverse primers. Ct values were normalized to the Ct values of 18S. Ct values from experimental treatments were subtracted from

control treatments to calculate a delta Ct value. A delta-delta CT value was then calculated using the formula $2^{-\Delta\Delta Ct}$. Delta-delta CT values were then transformed by Log2. Graphs of these results were created using PRISM V10.

Immunofluorescent Staining. Competent larvae fed for 36 h with bacteria carrying dsRNA plasmids pDS-CA1, pDS- α tubulin, or pDS-gfp were treated with 7.5% MgCl and washed three times in ASW. Larvae were then fixed overnight in 4% PFA at 4 °C. Larvae were washed three times in PBS + 1% Triton X (PBT) and pretreated in PBT with 10% Goat Serum (Fisher 16210064) for 1 h. Anti- α tubulin 1:1,000 (Rockland 600-401-880S) primary antibody was then added at a 1:100 dilution to PBT with 10% Goat Serum and incubated overnight. Samples were then washed 3 \times in PBT for 10 min and resuspended in a 1:100 dilution of DyLight 555 secondary anti-goat anti-rabbit antibody (Fisher A-21428) with blocking buffer (PBT + 10% Goat Serum) for 1 h. Samples were then washed 3 \times in PBT for 10 min each and mounted in ProLong Antifade Diamond Mountant with DAPI (Molecular Probes P36961) at room temperature. Samples were imaged the same day on a Stellaris Leica Confocal using a 63 \times oil objective. Thirty larvae were counted for α tubulin expression and averaged within each treatment. The experiment was repeated three times with three different biological replicates (n = 3). Data were then analyzed using a chi-square with Yates' correction and then graphed using PRISM v10.

P. aeruginosa Infection. *P. aeruginosa* PA14 was struck out on an LB plate and grown for 24 h at 37 °C. A single colony was inoculated into a 5 mL culture of LB and cultured at 200 rpm at 37 °C for 18 h. The culture was then spun down at 4,000 rpm for 10 min and the pellet was washed with ASW. This was repeated three times to effectively transfer bacteria from LB media to ASW. The pellet was then resuspended in 1 mL of ASW. The bacteria were diluted to an OD of 3, and a serial dilution was made in a 96-well plate containing larvae that were pretreated with ASW, pDS-MyD88, or pDS-gfp for 24 h. Larvae survival was quantified in triplicate wells for replication every 2 h for 8 h. Survival was averaged by three technical replicates. The experiment was repeated three times with three biological replicates (n = 3). A one-way ANOVA was performed against all six treatments at each individual OD averaged across the 8 h. To compare similarity across each treatment, a Tukey post hoc test was performed. Data were analyzed using PRISM v10 and graphed using R studio 4.3.3.

Hybridization Chain Reaction. Whole mount embryo HCRs were carried out as described in ref. 70 in 1.5 mL tubes. *MyD88*, *CA1*, and *atubulin* probes were designed by Molecular Instruments using mRNA coding sequences from *Hydroides* transcriptome. *RUNX*, *IL17*, *Fos*, and *NHR2* probes were designed in Python using in situ probe generator v.0.3.2 (71). Amplifiers and probe washing buffers were purchased from Molecular Instruments. Larvae were exposed to a 1:100 dilution of MACs extracts for 5 and 30 min. Larvae were then treated in 6.5%

MgCl to relax larvae and then washed twice with ASW. Larvae were fixed in 4% PFA (2.5 mL 16% PFA, 1 mL 10 \times PBS Buffer, 6.5 mL RNase free H₂O) overnight at 4 °C on a nutator. Samples were washed in 5 \times SSCT (10 mL of 20 \times saline sodium citrate (SSC), 400 μ L 10% Tween 20, 44.5 mL RNase free H₂O) and probes were added to hybridization buffer at a concentration of 1 pM per gene. Samples were prehybridized for 30 min at 37 °C before probes were added. The following day, samples were washed four times in intervals of 30 min with probe wash buffer. Hairpins were heat shocked at 95 °C for 90 s and snap cooled for 30 min at room temperature. Hairpins and amplifier buffer were added to samples and incubated overnight at 37 °C. The following day, samples were washed four times with 5 \times SSCT in 30-min intervals and mounted in ProLong Antifade Diamond Mountant with DAPI (Molecular Probes P36961). Samples were imaged the same day on a Stellaris Leica Confocal using a 63 \times oil objective. Fluorescence was determined by scanning the larval z-stack and setting gain and intensity at the lowest exposure time where fluorescence was present throughout the animal. For graphs representing counts of HCR expression, larvae that had no fluorescence were counted as larvae that have "no expression." If a larvae had any fluorescence that was present after autofluorescence was removed, that larvae would be counted to have "expression." The total number of larvae that were counted as expression were reported out of the total number of larvae (n = 30) and repeated in three technical replicates. Data were then averaged across three biological replicates and analyzed using a chi-square test with Yates' correction in PRISM v10.

Data, Materials, and Software Availability. Imaging data (confocal, fluorescence, DIC) generated for this manuscript are freely available in Figshare (<https://doi.org/10.6084/m9.figshare.c.7705664>) (72). All other data are included in the manuscript and/or *SI Appendix*.

ACKNOWLEDGMENTS. We thank Dr. Ricardo Zayas and the members of the Shikuma Lab for their constructive comments on the manuscript. We thank Dr. Stanley Maloy, Dr. Lisa Racki, and Dr. Alison Gould for gifting us bacterial strains used in this work. This work was supported by the NSF (1942251, N.J.S.), the Gordon and Betty Moore Foundation (GBMF9344, N.J.S.; <https://doi.org/10.37807/GBMF9344>), Office of Naval Research (N00014-20-1-2120 to N.J.S.), the NIH, NIGMS (R35GM146722, N.J.S.) and the Alfred P. Sloan Foundation, Sloan Research Fellowship (N.J.S.). E.D. and M.V.F. are fellows of the Rees-Stealy Research Foundation.

Author affiliations: *Department of Biology and Viral Information Institute, San Diego State University, San Diego, CA 92182

Author contributions: E.D., M.V.F., and N.J.S. designed research; E.D., M.V.F., T.N.A., J.R.A., and K.E.M. performed research; E.D., M.V.F., and N.J.S. analyzed data; and E.D., M.V.F., and N.J.S. wrote the paper.

1. S. F. Gilbert, T. C. G. Bosch, C. Ledón-Rettig, Eco-evo-devo: Developmental symbiosis and developmental plasticity as evolutionary agents. *Nat. Rev. Genet.* **16**, 611–622 (2015).
2. B. R. Schmidt, W. Hödl, M. Schaub, From metamorphosis to maturity in complex life cycles: Equal performance of different juvenile life history pathways. *Ecology* **93**, 657–667 (2012).
3. K. M. Warkentin, Environmentally cued hatching across taxa: Embryos respond to risk and opportunity. *Integr. Comp. Biol.* **51**, 14–25 (2011).
4. J. H. Hill *et al.*, BefaA, a microbiota-secreted membrane disrupter, disseminates to the pancreas and increases β cell mass. *Cell Metab.* **34**, 1779–1791.e9 (2022).
5. A. Mishra *et al.*, Microbial exposure during early human development primes fetal immune cells. *Cell* **184**, 3394–3409.e20 (2021).
6. S. V. Nyholm, M. J. McFall-Ngai, A lasting symbiosis: How the Hawaiian bobtail squid finds and keeps its bioluminescent bacterial partner. *Nat. Rev. Microbiol.* **19**, 666–679 (2021).
7. C. E. Zobell, E. C. Allen, The significance of marine bacteria in the fouling of submerged surfaces. *J. Bacteriol.* **29**, 239–251 (1935).
8. G. S. Cavalcanti, A. T. Alker, N. Delherbe, K. E. Malter, N. J. Shikuma, The influence of bacteria on animal metamorphosis. *Annu. Rev. Microbiol.* **74**, 137–158 (2020).
9. M. G. Hadfield, Biofilms and marine invertebrate larvae: What bacteria produce that larvae use to choose settlement sites. *Annu. Rev. Mar. Sci.* **3**, 453–470 (2011).
10. B. Roberts *et al.*, A complement response may activate metamorphosis in the ascidian *Boltenia villosa*. *Dev. Genes Evol.* **217**, 449–458 (2007).
11. P. Balseiro, R. Moreira, R. Chamorro, A. Figueras, B. Novoa, Immune responses during the larval stages of *Mytilus galloprovincialis*: Metamorphosis alters immunocompetence, body shape and behavior. *Fish Shellfish Immunol.* **35**, 438–447 (2013).
12. B. Davidson, B. J. Swalla, A molecular analysis of ascidian metamorphosis reveals activation of an innate immune response. *Development* **129**, 4739–4751 (2002).
13. N. Siboni, D. Abrego, C. A. Motti, J. Tebben, T. Harder, Gene expression patterns during the early stages of chemically induced larval metamorphosis and settlement of the coral *Acropora millepora*. *PLoS ONE* **9**, e91082 (2014).
14. N. J. Shikuma, I. Antoshechkin, J. M. Medeiros, M. Pilhofer, D. K. Newman, Stepwise metamorphosis of the tubeworm *Hydroides elegans* is mediated by a bacterial inducer and MAPK signaling. *Proc. Natl. Acad. Sci. U.S.A.* **113**, 10097–10102 (2016).
15. J. T. Critchlow, A. Norris, A. T. Tate, The legacy of larval infection on immunological dynamics over metamorphosis. *Philos. Trans. R. Soc. Lond. B, Biol. Sci.* **374**, 20190066 (2019).
16. S. Natori, H. Shiraishi, S. Hori, A. Kobayashi, The roles of Sarcophaga defense molecules in immunity and metamorphosis. *Dev. Comp. Immunol.* **23**, 317–328 (1999).
17. S. Valanne, J.-H. Wang, M. Rämetsä, The *Drosophila* Toll signaling pathway. *J. Immunol.* **186**, 649–656 (2011).
18. S. Franzenburg *et al.*, MyD88-deficient Hydra reveal an ancient function of TLR signaling in sensing bacterial colonizers. *Proc. Natl. Acad. Sci. U.S.A.* **109**, 19374–19379 (2012).
19. S. Tauszig-Delamasure, H. Bilak, M. Capovilla, J. A. Hoffmann, J.-L. Imler, *Drosophila* MyD88 is required for the response to fungal and Gram-positive bacterial infections. *Nat. Immunol.* **3**, 91–97 (2002).
20. C. F. Ericson *et al.*, A contractile injection system stimulates tubeworm metamorphosis by translocating a proteinaceous effector. *eLife* **8**, e46845 (2019).
21. B. T. Nedved, M. G. Hadfield, *Hydroides elegans* (Annelida: Polychaeta): A Model for Biofouling Research (Springer, 2008), pp. 1–15.
22. N. J. Shikuma *et al.*, Marine tubeworm metamorphosis induced by arrays of bacterial phage tail-like structures. *Science* **343**, 529–533 (2014).
23. A. Grishok, RNAi mechanisms in *Caenorhabditis elegans*. *FEBS Lett.* **579**, 5932–5939 (2005).
24. P. A. Newmark, P. W. Reddien, F. Cebrià, A. S. Alvarado, Ingestion of bacterially expressed double-stranded RNA inhibits gene expression in planarians. *Proc. Natl. Acad. Sci. U.S.A.* **100**, 11861–11865 (2003).
25. L. Timmons, A. Fire, Specific interference by ingested dsRNA. *Nature* **395**, 854–854 (1998).
26. L. A. Gosselin, P.-Y. Qian, Can bacterivory sustain survival and growth in early juveniles of the bryozoan *Bugula neritina*, the polychaete *Hydroides elegans* and the barnacle *Balanus amphitrite*? *Mar. Ecol. Prog. Ser.* **192**, 163–172 (2000).

27. A. L. Gould, J. B. Henderson, Comparative genomics of symbiotic *Photobacterium* using highly contiguous genome assemblies from long read sequences. *Microb. Genomics* **9**, 001161 (2023).
28. K. T. Nesbit, N. J. Shikuma, Future research directions of the model marine tubeworm *Hydroides elegans* and synthesis of developmental staging of the complete life cycle. *Dev. Dyn.* **252**, 1391–1400 (2023).
29. L. Timmons, D. L. Court, A. Fire, Ingestion of bacterially expressed dsRNAs can produce specific and potent genetic interference in *Caenorhabditis elegans*. *Gene* **263**, 103–112 (2001).
30. A. T. Alker *et al.*, A modular plasmid toolkit applied in marine bacteria reveals functional insights during bacteria-stimulated metamorphosis. *mBio* **14**, e01502–23 (2023).
31. S. P. Leonard *et al.*, Genetic engineering of bee gut microbiome bacteria with a toolkit for modular assembly of broad-host-range plasmids. *ACS Synth. Biol.* **7**, 1279–1290 (2018).
32. S. P. Leonard *et al.*, Engineered symbionts activate honey bee immunity and limit pathogens. *Science* **367**, 573–576 (2020).
33. G. Batzel, B. T. Nedved, M. G. Hadfield, Expression and localization of carbonic anhydrase genes in the serpulid polychaete *Hydroides elegans*. *Biol. Bull.* **231**, 175–184 (2016).
34. L. Xie *et al.*, Targeting of MyD88 homodimerization by novel synthetic inhibitor TJ-M2010-5 in preventing colitis-associated colorectal cancer. *J. Natl. Cancer Inst.* **108**, djv364 (2016).
35. S.-H. Kim, S.-Y. Park, Y.-J. Heo, Y.-H. Cho, *Drosophila melanogaster*-based screening for multihost virulence factors of *Pseudomonas aeruginosa* PA14 and identification of a virulence-attenuating factor, HudA. *Infect. Immun.* **76**, 4152–4162 (2008).
36. J. M. Plotnikova, L. G. Rahme, F. M. Ausubel, Pathogenesis of the human opportunistic pathogen *Pseudomonas aeruginosa* PA14 in *Arabidopsis*. *Plant Physiology* **124**, 1766–1774 (2000).
37. M.-W. Tan, S. Mahajan-Miklos, F. M. Ausubel, Killing of *Caenorhabditis elegans* by *Pseudomonas aeruginosa* used to model mammalian bacterial pathogenesis. *Proc. Natl. Acad. Sci. U.S.A.* **96**, 715–720 (1999).
38. N. J. Shikuma, Bacteria-stimulated metamorphosis: An ocean of insights from investigating a transient host-microbe interaction. *Interaction. mSystems* **6**, e0075421 (2021), 10.1128/mSystems.00754-21.
39. B. Altincicek, A. Vilcinskas, Metamorphosis and collagen-IV-fragments stimulate innate immune response in the greater wax moth, *Galleria mellonella*. *Dev. Comp. Immunol.* **30**, 1108–1118 (2006).
40. N. Pollet, Expression of immune genes during metamorphosis of *Xenopus*: A survey. *Front. Biosci.* **15**, 348–358 (2010).
41. J. T. Xiao Joe *et al.*, The microbiota profile and transcriptome analysis of immune response during metamorphosis stages in orange spotted grouper (*Epinephelus coioides*). *Fish Shellfish Immunol.* **90**, 141–149 (2019).
42. H. Sun, P. Towb, D. N. Chiemi, B. A. Foster, S. A. Wasserman, Regulated assembly of the Toll signaling complex drives *Drosophila* dorsoventral patterning. *EMBO J.* **23**, 100–110 (2004).
43. P. Schroeder *et al.*, Abnormal brain structure and behavior in MyD88-deficient mice. *Brain Behav. Immun.* **91**, 181–193 (2021).
44. K. M. Buckley *et al.*, IL17 factors are early regulators in the gut epithelium during inflammatory response to *Vibrio* in the sea urchin larva. *eLife* **6**, e23481 (2017).
45. A. Cerami, Inflammatory cytokines. *Clin. Immunol. Immunopathol.* **62**, S3–S10 (1992).
46. R. Choghakhorji, A. Abbasnezhad, A. Hasanvand, R. Amani, Inflammatory cytokines and oxidative stress biomarkers in irritable bowel syndrome: Association with digestive symptoms and quality of life. *Cytokine* **93**, 34–43 (2017).
47. J. Hawiger, Innate immunity and inflammation: A transcriptional paradigm. *Immunol. Res.* **23**, 99–109 (2001).
48. F. Bejjani, E. Evanno, K. Zibara, M. Piechaczyk, I. Jariel-Encontre, The AP-1 transcriptional complex: Local switch or remote command? *Biochim. Biophys. Acta: Rev. Cancer* **1872**, 11–23 (2019).
49. K. A. Lord, A. Abdollahi, B. Hoffman-Liebermann, D. A. Liebermann, Proto-oncogenes of the Fos/Jun family of transcription factors are positive regulators of myeloid differentiation. *Mol. Cell. Biol.* **13**, 841–851 (1993).
50. G. A. Preston *et al.*, Induction of apoptosis by c-Fos protein. *Mol. Cell. Biol.* **16**, 211–218 (1996).
51. J. Canon, U. Banerjee, Runt and lozenge function in *Drosophila* development. *Semin. Cell Dev. Biol.* **11**, 327–336 (2000).
52. J. C. Wheeler, K. Shigesada, J. Peter Gergen, Y. Ito, Mechanisms of transcriptional regulation by Runt domain proteins. *Semin. Cell Dev. Biol.* **11**, 369–375 (2000).
53. K. E. Malter *et al.*, Diacylglycerol, PKC and MAPK signaling initiate tubeworm metamorphosis in response to bacteria. *Dev. Biol.* **487**, 99–109 (2022).
54. A. Aranda, A. Pascual, Nuclear hormone receptors and gene expression. *Physiol. Rev.* **81**, 1269–1304 (2001).
55. K. E. Malter *et al.*, A bacterial membrane-disrupting protein stimulates animal metamorphosis. *mBio* **16**, e03573–24 (2024).
56. K. Hao, Y. Chen, X. Yan, X. Zhu, Cilia locally synthesize proteins to sustain their ultrastructure and functions. *Nat. Commun.* **12**, 6971 (2021).
57. J. P. Brandt, N. Ringstad, Toll-like receptor signaling promotes development and function of sensory neurons required for a *C. elegans* pathogen-avoidance behavior. *Curr. Biol.* **25**, 2228–2237 (2015).
58. O. W. Liu, K. Shen, The transmembrane LRR protein DMA-1 promotes dendrite branching and growth in *C. elegans*. *Nat. Neurosci.* **15**, 57–63 (2012).
59. B. Barak, N. Feldman, E. Okun, Toll-like receptors as developmental tools that regulate neurogenesis during development: An update. *Front. Neurosci.* **8**, 272 (2014).
60. J. Lee *et al.*, Maintenance of colonic homeostasis by distinctive apical TLR9 signalling in intestinal epithelial cells. *Nat. Cell Biol.* **8**, 1327–1336 (2006).
61. J. M. Bates, J. Akerlund, E. Mittag, K. Guillemin, Intestinal alkaline phosphatase detoxifies lipopolysaccharide and prevents inflammation in zebrafish in response to the gut microbiota. *Cell Host Microbe* **2**, 371–382 (2007).
62. M. Bakula, The persistence of a microbial flora during postembryogenesis of *Drosophila melanogaster*. *J. Invertebr. Pathol.* **14**, 365–374 (1969).
63. T. Brummel, A. Ching, L. Seroude, A. F. Simon, S. Benzer, *Drosophila* lifespan enhancement by exogenous bacteria. *Proc. Natl. Acad. Sci. U.S.A.* **101**, 12974–12979 (2004).
64. C. M. Hammell, G. J. Hannon, Inducing RNAi in *C. elegans* by feeding with dsRNA-expressing *E. coli*. *Cold Spring Harb. Protoc.* **2012**, pdb.prot072348 (2012).
65. N. Kunte, E. McGraw, S. Bell, D. Held, L.-A. Avila, Prospects, challenges and current status of RNAi through insect feeding. *Pest Manage. Sci.* **76**, 26–41 (2020).
66. R. Katoch, A. Sethi, N. Thakur, L. L. Murdock, RNAi for insect control: Current perspective and future challenges. *Appl. Biochem. Biotechnol.* **171**, 847–873 (2013).
67. C. R. Davidson, N. M. Best, J. W. Francis, E. L. Cooper, T. C. Wood, Toll-like receptor genes (TLRs) from *Capitella capitata* and *Helobdella robusta* (Annelida). *Dev. Comp. Immunol.* **32**, 608–612 (2008).
68. A. T. Alker *et al.*, Linking bacterial tetrabromopyrrole biosynthesis to coral metamorphosis. *ISME Commun.* **3**, 1–4 (2023).
69. I. Rocchi *et al.*, A bacterial phage tail-like structure kills eukaryotic cells by injecting a nuclease effector. *Cell Rep.* **28**, 295–301.e4 (2019).
70. H. M. T. Choi, V. A. Beck, N. A. Pierce, Next-generation in situ hybridization chain reaction: Higher gain, lower cost, greater durability. *ACS Nano* **8**, 4284–4294 (2014).
71. E. Kuehn *et al.*, Segment number threshold determines juvenile onset of germline cluster expansion in *Platynereis dumerilii*. *J. Exp. Zool., Part B: Mol. Dev. Evol.* **338**, 225–240 (2022).
72. E. Darin, M. Farrell, N. Shikuma, MyD88 knockdown by RNAi prevents bacterial induction of tubeworm metamorphosis. Figshare. <https://doi.org/10.6084/m9.figshare.c.7705664.v1>. Deposited 13 May 2025.